On the difficulty of interpreting NO-LIF measurements around 226 nm in confined ammonia flames

Nour El Baba, Pascale Desgroux, Nathalie Lamoureux

Combustion and Flame 264 (2024) 113424

Contents lists available at ScienceDirect

Combustion and Flame

journal homepage: www.sciencedirect.com/journal/combustion-and-flame

On the difficulty of interpreting NO-LIF measurements around 226 nm in confined ammonia flames

Nour El Baba, Pascale Desgroux, Nathalie Lamoureux *

CNRS, UMR 8522, PC2A - Physicochimie des Processus de Combustion et de l'Atmosphère, Université de Lille, Lille F-59000, France

ARTICLE INFO

Keywords:
NO-LIF
NH_3
Absorption
Thermometry

ABSTRACT

This paper addresses how NH_3 and NO absorption along the laser axis disrupts NO-LIF measurements made around 225 nm in $NH_3/O_2/N_2$ premixed flames confined at low pressure (10 kPa). Measurements were performed in 3 flames (equivalence ratio ϕ = 0.87, 1.1 and 1.3) with 24 % N_2 dilution. Together with the LIF measurements, single-pass absorption measurements were obtained in all flames as a function of the height above the burner (HAB) and of the wavelength. A significant NH_3 absorption of the laser beam is found in the pre-heat zone and flame front of each flame, as well as in the burned gas in the rich flame. In the lean flame, whatever the HAB, an additional significant absorption is due to the NO present in the gas surrounding the flame. Whereas NH_3 absorbance only occurs inside the flame under all conditions, NO absorbance is mainly due to the high concentration of NO produced in the lean flame and spread in the entire confined vessel around the flame. From this analysis, relative NO rotational population profiles were recorded by measuring the temporal peak of the LIF signals (prompt-LIF) which were corrected for absorption to account for the available energy at burner's center. NO-LIF thermometry was conducted to determine the temperature in the flames through collecting excitation LIF spectra and performing spectral fitting using a dedicated software (thermo NO-LIF, https://pc2a.univ-lille.fr/thermo-no-lif/). The procedure developed to collect the NO profiles could not be transposed to determine the temperature in the lean flame. Indeed, the attenuation of the laser beam depends on whether the laser is tuned on a "cold" transition (strongly impacted by absorption outside the flame) or on a "hot" transition of NO, little affected. Thus, two tubes (with N_2 flushing) were installed inside the vessel along the laser axis and surrounding the flame to suppress the NO absorbance.

1. Introduction

Ammonia as H_2 carrier and free-carbon molecule is a good candidate to fulfil the transition to low-carbon energy. However, there are some issues using NH_3 as fuel in combustion application because NO_x emissions and unburned NH_3 release can be important under lean and rich conditions, respectively. Although ammonia combustion does not give rise to CO_2 emissions, the production of NO_x and N_2O (greenhouse gas with a potential effect 265 times higher than CO_2) emissions caused by its N-containing is another barrier that must be overcome, owing to the fact that these emissions induce the acid rain and the depletion of the ozone layer [1,2].

As NH_3 has a very low energy density compared to fossil fuel (around 40 % less), it is generally used in combustion as a blend with either hydrocarbon, oxygenated fuels or H_2 (added or from partial cracking of NH_3). In order to reach a laminar burning velocity compatible with a stable flame of pure NH_3, it is possible to burn it in O_2-enriched atmosphere [3]. In ammonia oxidation, the NO_x formation follows the fuel-NO pathway, but as the temperature increases with the O_2 enhancement, the thermal-NO pathway can also be important. To elucidate the reaction pathways of NO_x formation during NH_3 oxidation, it is valuable to scrutinize species profiles as a function of temperature in jet-stirred or plug-flow reactors [4–6], or as a function of distance in flat laminar flames [7–16]. Some studies have been performed in shock tube apparatus where temporal NO species profiles are measured [17,18]. The measurement of the NO species in absolute concentration is crucial and can be performed after gas probe sampling using gas analyzer, Fourier Transformed Infra-Red spectroscopy and Molecular Beam Mass Spectrometry. The advantage of spectroscopic laser diagnostics as Laser Induced Fluorescence (LIF) and absorption is the possibility to measure *in situ* and instantaneously NO species without perturbation even in turbulent combustion. In addition, temperature can be obtained using

* Corresponding author.
E-mail address: nathalie.lamoureux@univ-lille.fr (N. Lamoureux).

https://doi.org/10.1016/j.combustflame.2024.113424
Received 24 October 2023; Received in revised form 14 March 2024; Accepted 14 March 2024
Available online 25 March 2024

multi-line LIF thermometry [19,20].

Strategies for LIF detection of NO were scrutinized by Bessler et al. [21–23] in hydrocarbon flames. The authors described the advantages/drawbacks of probing NO along the $A^2\Sigma^+$-$X^2\Pi(0,0)$ or $A^2\Sigma^+$-$X^2\Pi(0,1)$ bands at pressure equal to or higher than 100 kPa. Absorption from NH_3, H_2O, CO_2 and spectral interferences from O_2 LIF (Schumann-Runge bands) and broadband fluorescence (PAH) are mentioned to be an issue for NO LIF in the UV range. Selection of narrow bandwidth of collection allows to restrict the interference from O_2 LIF. NO measurements are preferentially obtained by probing a transition line whose rotational population in the ground state has a weakly temperature dependent Boltzmann factor as line $Q_2(26.5)$ in a standard flame temperature range [24–27]. Such measurements are frequently conducted by exciting the vibrational $v" = 0$ of the ground state X, because more than 74 % of the population belongs to this level at $T = 2000$ K.

Chou et al. [8] performed one of the first LIF and absorption measurements of NO in ammonia flames stabilized at atmospheric pressure above a McKenna burner. NO LIF signals were converted into absolute mole fractions using absorption measurements along the $A^2\Sigma^+$-$X^2\Pi(0,0)$ band (around 226.8 nm). In rich flame conditions ($\phi = 1.5$), the authors reported difficulties during NO LIF measurements because of the strong attenuation of the laser (about 99.9 % at 0.6 mm and 35 % at 6 mm above the burner). Note that the low nitrogen dilution (less than 12 % in vol.) of the investigated flames may have enhanced the impact of NH_3 absorption. Even in the leanest flame condition ($\phi = 0.5$), the absorption spectrum presents not only structured transitions of NO but also a continuum absorption attributed to NH_3 [28,29]. Brackmann et al. [12] measured NO using LIF in atmospheric premixed NH_3/air flames above a McKenna burner ($0.9 < \phi < 1.2$). The absolute quantification of NO was conducted using the bi-directional excitation LIF technique described in [30]. This efficient technique allows species quantification provided that no other species absorbs in the same spectral range as the target species. In [12], NO was measured by exciting the $Q_1(23.5)$ $A^2\Sigma^+$-$X^2\Pi(0,0)$ transition, with no indication that this line was overlapped by the $P_1(31.5)$ line. No other interference is mentioned. Other studies [13,31,32] were conducted at atmospheric conditions in flames using planar NO LIF but none of them reported difficulties due to NH_3 or NO absorption.

To significantly reduce the NH_3 absorption around 225 nm, Chou et al. [8] measured the absolute concentration of NO using LIF and absorption in the $A^2\Sigma^+$-$X^2\Pi(0,1)$ band at 237.5 nm. Despite the LIF signals were reduced by about a factor of 2.5 compared to the ones performed at 226 nm, a satisfying signal to noise ratio (SNR) could be achieved. Recently, Wang et al. [33] selected the $A^2\Sigma^+$-$X^2\Pi(0,1)$ band to perform quantitative NO LIF measurements in $NH_3/H_2/N_2$ turbulent jet flames at 5 bar. The quantification of the LIF signal in absolute mole fraction of NO was realized in a laminar H_2/N_2 counterflow diffusion flame using a standard addition method. Because of the elevated pressure, the interferences due to O_2 had to be corrected in order to improve the ratio NO/O_2 LIF as reported in [34].

Dean et al. [35] measured NH_3 concentration profiles of atmospheric NH_3/O_2 flames using laser absorption at 230 nm. Yang et al. [36] conducted broadband absorption measurements of multi species including NO and NH_3 around 225 nm in atmospheric premixed ammonia/methane/air flames. They could derive the respective contribution of NO, NH_3 and CO_2 absorbances. Despite the recent work of Weng et al. [37], there is still a lack of data for NH_3 absorption cross section at high temperature which prevent Yang et al. [36] to determine the NH_3 absolute concentration. During the publication process, the authors became aware of the measurement of the NH_3 absorption cross-section performed in shock tube over a T range of 1750 to 2500 K by Rault et al. [38]. These results are not integrated in the rest of this paper.

In confined environment, either at low pressure or at high pressure, the expected high level of NO density (from a few tenths to a few percent) combined with the high density of NH_3 can result in spectral absorption interferences around 225 nm as earlier mentioned [8,36]. Contrary to NH_3 which is spectrally characterized by a quasi-continuum, NO presents a structured rotational spectrum. Note that both molecules are stable and can be present in the confined gases surrounding the flame. Also, NH_3 as a fuel is consumed locally in the flame yielding NO. Large amounts of NO surrounding the flame and confined in the vessel may interfere with the NO-LIF measurements due to absorption [39]. Pillier et al. [40] conducted NO absorption measurements using Cavity Ring-Down Spectroscopy (CRDS) in low-pressure methane flames. Due to the recirculation of the burned gases in the low-pressure enclosure, absorption along the line-of-sight involves not only NO present in the flame at high temperature but also NO in the surrounding gas at colder temperature. The additional absorption found in the $A^2\Sigma^+$-$X^2\Pi(0,0)$ band prevented that reliable absorption measurements of NO could be performed, therefore the $A^2\Sigma^+$-$X^2\Pi(0,1)$ band needed to be selected.

Analysis of the literature shows that the perturbation of NO measurement caused by the presence of ammonia depends on the type of flame studied. This disturbance is amplified in confined enclosures by the additional absorption due to NO present around the flame. In such situations, switching to the $A^2\Sigma^+$-$X^2\Pi(0,1)$ band is an interesting strategy for measuring NO, although the measurements are much more sensitive to temperature. On the other hand, measuring temperature by probing different rotational lines from the level $v" = 1$ by LIF is not accurate enough due to its high-temperature feature. To the best of our knowledge, no attempt for NO-LIF thermometry has been conducted in ammonia flames.

In this work, LIF and absorption diagnostics were conducted in $NH_3/O_2/N_2$ flames at low-pressure (10 kPa) for measuring temperature, and NO profiles along the flame axis. We investigate how to combine temperature measurement by NO-LIF thermometry and NO concentration measurement in a confined vessel by using the $A^2\Sigma^+$-$X^2\Pi(0,0)$ band. Temperature was determined from NO-LIF thermometry. The principle of LIF thermometry relies on the temperature dependence of the rotational population distribution of the target species. NO is a good candidate because its fluorescence quantum yield is independent of the rotational number [20,41]. NO-LIF measurements were affected by the absorption due to NO and NH_3. This absorption affects not only the absolute quantification (not presented here) but also the relative mole fraction of NO in between flames and along the vertical axis. The paper presents a detailed approach developed in order to circumvent the difficulties encountered around 225 nm in confined vessel due to the NO absorption in the "cold" area and also the NH_3 absorption all along the flame axis, in the lean and in the rich flame conditions respectively.

2. Experimental setup

2.1. Low pressure burner and gas supply

Experiments have been carried out in laminar $NH_3/O_2/N_2$ premixed flames stabilized above a 6-cm diameter stainless-steel water-cooled (at 323 K) McKenna burner (Holthuis & Associates). Volumetric flow rates of the gas mixture are regulated by using Mass Flow Controller (MFC, EL-FLOW except LOW-ΔP-FLOW for NH_3, Bronkhorst), see Table 1. Additionally, a nitrogen shroud was introduced through a rotameter (~ 0.2 slpm) to prevent corrosion of the bronze disc around the burner. Accurary of the MFCs is 1.0 %. The burner is movable in the vertical direction. The height above the burner (HAB) is defined by the distance between the laser axis and the burner surface. A picture of flame F1 is

Table 1
Flame conditions in mole fractions, equivalence ratio (ϕ), total flow rate is given in slpm unit (at 273.15 K and atmospheric pressure).

Flame	NH_3	O_2	N_2	ϕ	Total flow
F1	0.407	0.351	0.242	0.87	2.63
F2	0.454	0.311	0.235	1.1	2.71
F3	0.486	0.274	0.240	1.33	2.66

shown in Fig. 1.

A sketch of the experimental setup is shown in Fig. 1. The pressure enclosure is maintained at $p = 10$ kPa through an automatic regulator valve (F004BI, 300 NL/h, Bronkhorst) and a rotary-vacuum pump (NeoD25, Leybold). The steam water at the exhaust is trapped in a liquid N_2 vessel. The burner enclosure is equipped with different optical accesses allowing *in-situ* laser diagnostics (LIF and single-pass absorption). Additional details concerning the burner and gas supply are given in [27,41].

2.2. Laser diagnostics

The pulsed laser system consists of a frequency-doubled Nd:YAG laser (Quantel Q-smart) pumping a dye laser (Quantel TDL90+). Wavelengths around 226 nm (for probing NO in the $A^2\Sigma^+$-$X^2\Pi(0,0)$ band) are provided after doubling the fundamental dye radiation (around 572 nm) which is mixed with the Nd:YAG residual radiation at 1064 nm. The spectral laser bandwidth at 226 nm was estimated to be around 0.7 cm^{-1} [19]. The UV beam was separated using a step motorized pellin-broca in order to maintain constant the beam axis. The laser beam is introduced unfocused parallel to the burner surface. The laser intensity is controlled for each operating condition using 2 photodiodes (S1722, 1 ns-rise time, Hamamatsu), located after and before the burner enclosure, in order to measure the absorption along the radial axis. The LIF signal was collected at $f/6$ by 2 fused silica lenses ($f = 300$ mm) and focused onto the entrance slit of a spectrometer (SP2500i, $f/6.5$, Acton Research) with a 1200 gr/mm grating blazed at 300 nm. The output slit is adjusted to obtain a collection bandwidth of 9 nm, centered at 246 nm in order to collect the complete $A^2\Sigma^+$-$X^2\Pi(0–2)$ vibrational band of NO. Dispersed fluorescence spectra were measured at different HABs in all flames insuring that there were no O_2 LIF interferences. The emission was collected using a photomultiplier tube (XP2020Q, 1.5 ns rise-time, Photonis). The LIF and the photodiodes signals were recorded using a digital oscilloscope (HDO4000, 12-bit vertical resolution, 1 GHz bandwidth, 1.25 GS/s, LeCroy). During the acquisition of spectra, the dye laser wavelength was scanned at a rate equal to 0.5 pm/s and signals were continuously averaged over 10 laser shots. For the species profile measurements, signals are averaged over 300 laser pulses. Signals from the oscilloscope and the wavelength of the dye laser are transferred in real time on a PC, and treated with Labview programs.

The vertical resolution (z axis) is imposed by the image of the horizontal entrance slit of the spectrometer of 0.2 mm (z axis) and 10 mm (x axis), into the laser beam. To limit problems of scattering when we approach the burner surface, we have also limited the vertical size of the 6 mm diameter laser beam to 0.3 mm (z axis) with a slit placed on the laser axis (x axis). In addition, the size of the laser spot was limited to 1.5 mm in the y axis using a circular pinhole. Finally, the collection volume is a slab of 0.2 mm (z axis) × 10 mm (x axis) × 1.5 mm (y axis).

3. Techniques

3.1. Absorbance

Absorbance, $A(\bar{\nu})$, is measured according to the Beer-Lambert's law (Eq. (1)). Transmittance, $T(\bar{\nu})$, is equal to I_t/I_0, and absorption is equal to (1 - $T(\bar{\nu})$). I_t and I_0 were measured using 2 photodiodes located after and before the burner, respectively.

$$T(\bar{\nu}) = \frac{I_t}{I_0} = \exp(-k(\bar{\nu})l) = \exp(-A(\bar{\nu})) \quad (1)$$

$k(\bar{\nu})$, is the spectral absorption coefficient, $\bar{\nu}$ is the wavenumber and l is the absorption pathlength. The spectral absorption coefficient is equal to $\sigma(\bar{\nu}, T) \times [X]$. $\sigma(\bar{\nu}, T)$ is the integrated absorption cross section and [X] is the concentration of the X species. Thus, the absolute species concentration is derived from the absorbance measurement according to Eq. (2):

$$A(\bar{\nu}) = \sigma(\bar{\nu}, T)[X]l \quad (2)$$

Fig. 2a shows the laser axis inside the burner enclosure and the position of the 2 photodiodes outside the enclosure. The enclosure is ended with 2 windows 41 cm apart, corresponding to the entire absorption pathlength. At the central axis, the burner is vertically mobile. The flame is stabilized above the 6 cm diameter burner. The absorption pathlength crosses two distinct areas; the flame with a pathlength $l_F = 6$ cm and the surrounding gases with $l_S = 35$ cm (Fig. 2b). The transmittance standard deviation was determined to be lower than 1 %.

3.2. Laser-induced fluorescence

The prompt-LIF signal (S_{LIF}) is measured at the peak value of the temporal LIF signal. In the linear regime of fluorescence, the LIF signal is proportional to the rotational population of the laser-probed level, $N_{J''}$, according to Eq. (3).

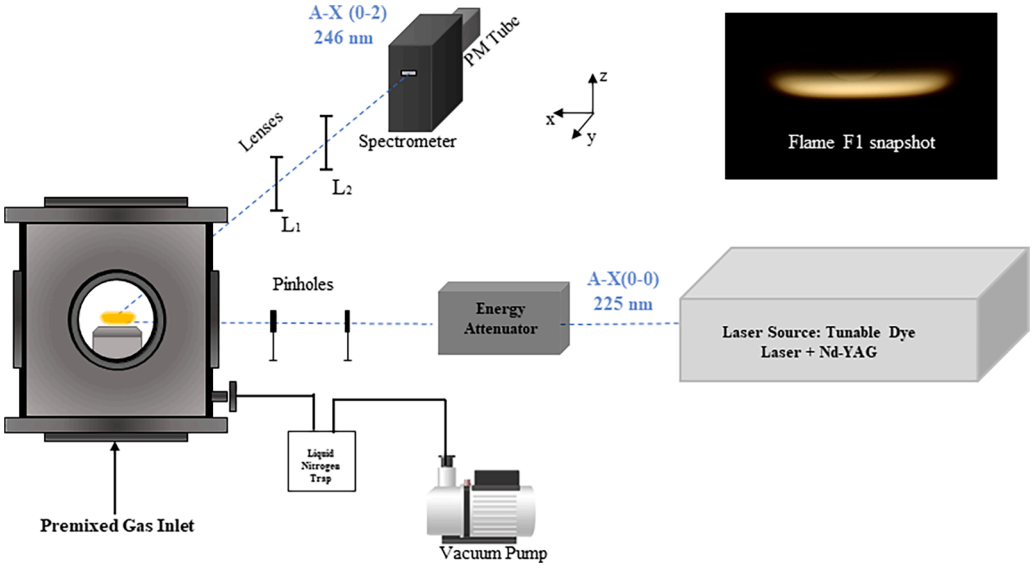

Fig. 1. Sketch of the experimental setup, with a snapshot of the F1 flame.

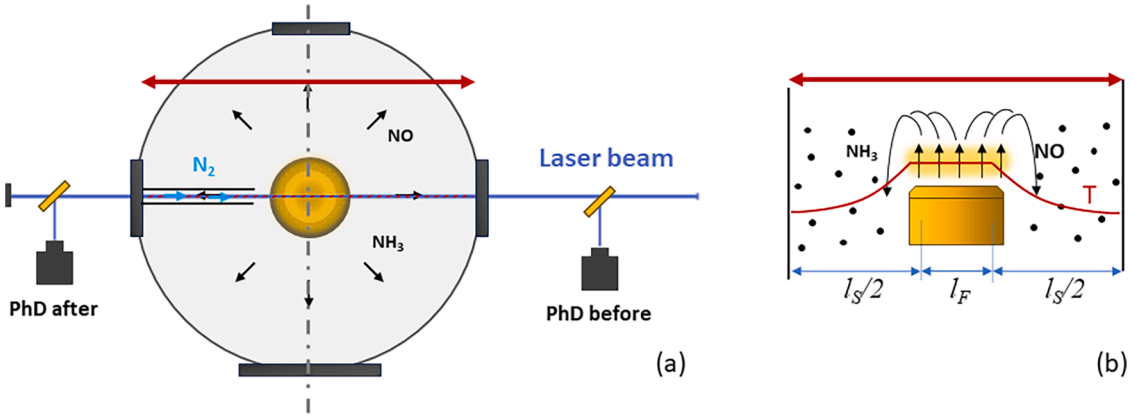

Fig. 2. Scheme of the absorption regions inside and outside the flame. (a) top view: the left-hand side represents the experimental device with the tube, the right-hand side without the tube. The tube use is specified in Section 4.3.2. (b) side view. The red arrows indicate the optical pathlength (41 cm) in the burner enclosure.

$$S_{\mathrm{LIF}} \propto N_{J''} \Phi I_L \quad (3)$$

Measurements are performed under controlled laser energy (I_L) in the probed volume, centered at the burner axis, to ensure being in the linear regime of fluorescence. Typically, the laser energy was equal to 1.5 mJ/cm^2 per pulse. In the investigated low-pressure flames, the LIF decay time is long enough relative to the laser pulse to ensure that prompt-LIF signals, measured at the temporal peak of the fluorescence, are unaffected by the variations of the fluorescence quantum yield, $\Phi = A/(A + Q)$. A is the emission Einstein coefficient and Q is the quenching rate. The Supplementary Materials (section A) reports measurements and their analysis allowing to confirm the validity of this assumption.

In order to limit the impact of the temperature uncertainties on the Boltzmann factor calculation ($f_B(J'',T)$), rotational number J" = 26.5 is selected for probing $Q_2(26.5)+R_{12}(26.5)$ transition of NO around 225.58 nm [24–27]. Mixing of these lines is inevitable in the case of NO, but they both originate from the same rotational level in the ground state, which facilitates interpretation of the LIF signal. In what follows, the $Q_2(26.5)$ transition alone is specified for simplicity. LIF signal was corrected for laser absorption (see Section 3.1) by considering the effective laser energy, I_L, available in the volume of measure [42]. I_L was obtained from the transmittance measurement according to $I_L = (I_0+I_t)/2 = I_0(1 + T)/2$. The standard deviation of the collected LIF signal was estimated to be equal to 5 %.

3.3. NO-LIF thermometry

The temperature is determined using multi-line NO-LIF thermometry by scanning the laser wavelength from 225.45 to 225.72 nm following the recommendations from [19,20,43]. The fluorescence signal is collected at 246 nm along the entire A-X(0,2) vibrational band. According to recommendations for improving the accuracy of T measurements using NO-LIF thermometry in low pressure flames [19], the laser linewidth was set at 0.7 cm^{-1}. Measurements were performed in the linear regime of LIF. Each transition is characterized by its absorption Einstein coefficient, its rotational population, $N_{J''}$, and the Boltzmann factor, $f_B(J'',T)$. Temperature is then determined using the thermo-NO-LIF software [44]. The software evaluates NO-LIF spectra and derive temperature measurements from the excitation fluorescence spectra collected at different HAB. More details about the method are given in [19].

4. Experimental results

4.1. Absorbance around 225.5 nm

As both NO and NH_3 species are stable, they can be present not only in the flame but also in the surrounding gases [39,40,45]. Due the configuration of the flat flame, it is in essence assumed that in the flame, the gases and temperature remain constant along the laser axis, while in the surrounding gases, T is decreasing from the flame to the windows (red curve shown in Fig. 2b, adapted from [40]). The absorbance measurements aimed to differentiate between the absorbance of both species and the area where they are absorbing.

Absorbance along the laser pathway was measured in all flames as function of HAB when the laser wavelength is tuned either on-resonance with the $Q_2(26.5)$ transition of NO at 225.58 nm or at 225.53 nm wavelength (off-resonance with NO). At 225.58 nm (closed symbols in Fig. 3a), absorbance increases from the burner surface to around 3 mm. In case of the richest flame F3, the absorbance reaches 72 % and then decreases in the burned gases reaching a plateau above 20 mm at around 18 %. The peak of absorbance decreases with the decrease of ϕ, while the plateau values in the burned gases are around 9 % and 5 % in Flames F1 and F2, respectively. When the laser wavelength is tuned off-resonance to the $Q_2(26.5)$ transition of NO, the collected absorbance is attributed to NH_3 only (open symbols in Fig. 3a). The absorbance is due to NH_3 present in the flame, but also perhaps, to a lesser extent, in the surrounding gases. The latter being limited as the NH_3 absorption cross section around 225 nm decreases with decreasing T [28,37]. In the F1 flame, the off-resonance absorbance profile in the burned gases is negligible indicating clearly that the absorbance, when the wavelength is tuned on-resonance, is due to NO. The increase of the off-resonance profile towards the burner surface is due to NH_3 absorbance. From the subtracted on-off absorbance profiles (Fig. 3b), the NO absorbance is nearly constant along the HAB, and vary from 9 % to 5 % in the F1 and F2 flames, and is almost negligible in the F3 flame. By contrast, the NH_3 absorbance (open symbols in Fig. 3a) peaks up to 72 %, 50 % and 45 % in the F3, F2, F1 flames. Note that measurements (on- and off-resonance) performed in stoichiometric methane/O_2/N_2 flame show no evidence of absorbance along the laser pathlength and the HAB.

4.1.1. NH_3 absorption

In rich flame F3, absorbance spectra were collected at HAB = 1 and 22 mm in an extended range of wavelengths from 223.75 to 227.5 nm as shown in Fig. 4. In this flame, absorbance is not due to NO as shown above (Fig. 3b), and was assumed to be due to NH_3. The spectra were collected by scanning the wavelength at 5 pm/s with a continuous averaging of the signals over 10 laser shots. As will be described in Section 4.3.1, temperature was determined to be equal to 800 K at 1 mm

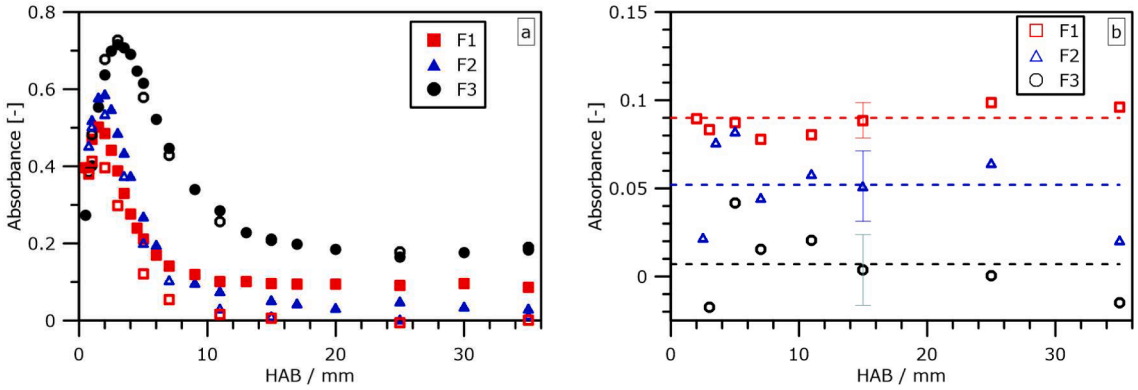

Fig. 3. Absorbance along the horizontal optical path as a function of HAB in flames $NH_3/O_2/N_2$. Flame conditions are given Table 1. a/ Laser wavelength was alternately tuned on resonance with $Q_2(26.5)$ transition of NO (closed symbols), and off-resonance (open symbols). b/ absorbance due to NO, with the average value along HAB (dashed lines).

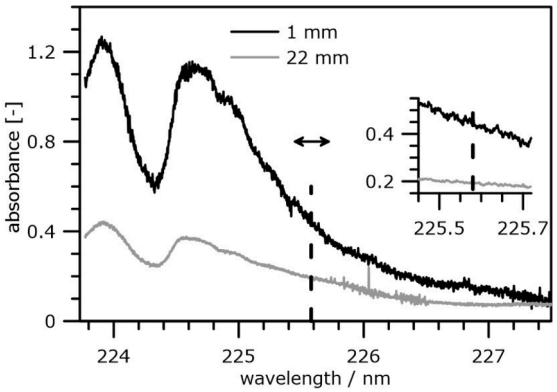

Fig. 4. Absorbance spectra obtained without tubes in the rich flame F3 at HAB =1 and 22 mm. The vertical dashed bar indicates the wavelength of $Q_2(26.5)$ transition of NO, the horizontal arrow the wavelength range scanned for thermometry measurements. Insert shows a magnification of the variation of the absorbance in the wavelength range used for LIF thermometry.

(the closest HAB where measurements were performed), and 2100 K at 22 mm, allowing to scrutinize a wide range of T and of amount of NH_3 in the flame. Absorbance values ($NO+NH_3$) when the wavelength is on-resonance with the $Q_2(26.5)$ transition of NO (at 225.58 nm, illustrated by the vertical dashed bar) are equal to 44 % and 19 % respectively at 1 and 22 nm, in agreement with Fig. 3a (closed circles).

It is well known that the NH_3 absorption spectrum is characterized at room T by an umbrella structure from 170 to 220 nm which spreads to higher wavelengths with T increase since higher vibronic levels of the ground state are populated [28,46]. However, only rare experimental data [37,47] are reported in the literature which limit the improvement of the spectral simulation of NH_3 around 225 nm with the increase of T. In this work, ammonia spectra were simulated using PGOPHER program [48]. Ro-vibronic spectroscopic constants and energy values are reported in Tables S2 and S3 of the Supplementary Materials (Section B). NH_3 molecule is non-planar (C_{3v} configuration) in its ground state, and planar in the electronic excited state (D_{3h} configuration). The umbrella of the spectrum is due to the progression of the N atom towards the plane defined by the H atoms, corresponding to the ν_2 mode of vibration of NH_3. The band structure appears to be characterized by the extended progression in the ν_2 mode of the $\tilde{A}$ excited state. Vibrational energy values of the $\nu''_2 = 0$, 1, 2 and 3 of the ground state $\tilde{X}$ were adopted from Huang et al. [49]. The ν''_2 mode is splitted into two levels, the lowest one being symmetric (s), the other antisymmetric (a). For instance, the splitting yields an energy gap of 284.71 cm^{-1} for the level $\nu''_2 = 2$. Spectral simulation performed with PGOPHER in [37] did not consider this splitting [50]. The values of B_v and C_v were extracted from [51,52]. The spectroscopic constants of the $\tilde{A}$ excited state were extracted from Ziegler [53]. The relative intensity of the vibrational band were adopted according to the Franck-Condon values, $q_{v'v''}$, from Harshbarger [54]. As the oscillator strength in PGOPHER is introduced as $\sqrt{q_{v'v''}}R_e$, the final values of the oscillator strength were adjusted at 298 K according to the NH_3 absorption cross section spectrum measured by Cheng et al. [55] (see Tables S4 and S5, and Fig. S1). Thus, R_e was implicitly assumed constant and equal to 0.173 Debye. Table 2 reports the comparison of the absorption cross sections at room T between the present simulation and the experimental ones [37,46,55]. Finally, PGOPHER simulation needs to be corrected for the actual vibrational partition function, Q_v, to calculate the absorption cross section [48,56]. Indeed, PGOPHER takes into consideration the partition function of the simulated vibronic levels of the ground state, meaning that the absorption spectrum has to be scaled by a ratio $Q_{v\ \mathrm{PGOPHER}}/Q_v$ where Q_v is the overall partition function. Therefore, both $Q_v(T)$ values were calculated using "vibrational spectrum" simulation in PGOPHER knowing the vibrational frequencies of NH_3 according to Zhu et al. [57] (see Table S6). For instance, the scaling ratio $Q_{v\ \mathrm{PGOPHER}}/Q_v$ is equal to 0.982, 0.945, and 0.534 at T = 590, 800 and 2100 K, respectively. This correction for Q_v was not considered in [37], according to [50]. The simulated absorption were found in good agreement with spectra measured by Weng et al. [37] from room temperature to 590 K (see Figs. S1 and S2). The PGOPHER input file is provided as Supplementary Materials.

Fig. 5 shows the comparison of the absorbance spectra measured at 1 mm and 22 mm in the F3 flame with the simulated absorption cross section spectrum at T = 800 K and 2100 K, respectively. The peaks at 224 and 224.6 nm correspond to the R-branch and $Q+P$-branches of the $\nu''_2 = 2$ band of NH_3. The experimental spectrum is reported in absorbance (left *Y-axis*), and the simulated spectrum is reported in absorption cross section, $\sigma(\bar{\nu}, T)$ (right *Y-axis*). Near the burner, a satisfying matching between the experimental spectrum and the calculated one is

Table 2
Absorption cross-section, σ, (10^{-18} cm^{-1}/(molec.cm^{-3})) at the peak wavelength of the $\tilde{A}(0,\nu_2,0,0)$- $\tilde{X}(0,0,0,0)$ transitions of NH_3 at 298 K. Comparison of the present determination with previous studies [37,46,55].

	0	1	2	3	4	5	6
σ^a	0.89	2.74	7.08	12.6	17.9	21	19.8
σ^b	1.00	3.52	8.11	12.8	17.4	19.9	20
σ^c	0.9	3.42	8.24	12.46	17.1	19.58	20.04
σ^d	1.38	3.88	8.64	12.86	16.99	19.28	19.65

[a] Present work.
[b] From Cheng et al. [55].
[c] From Limaõ-Vieira et al. [46].
[d] Extracted from simulation by Weng et al. [37].

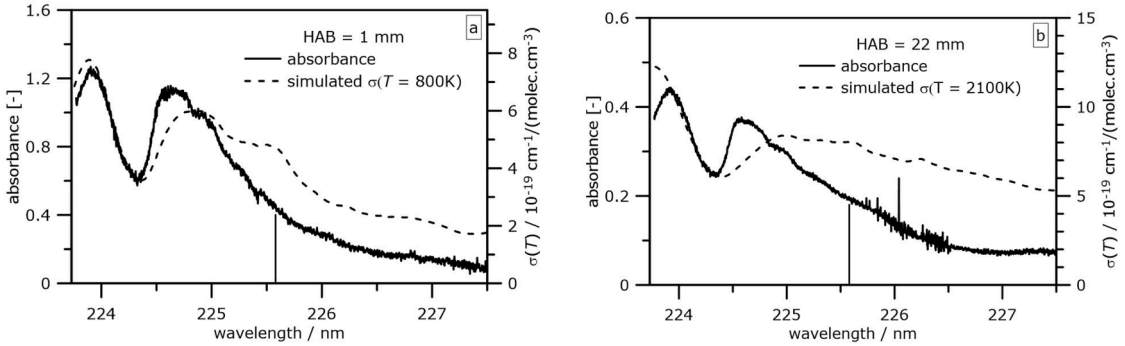

Fig. 5. Comparison of NH_3 absorbance spectrum measured in the F3 flame and the simulated absorption cross section using PGOPHER [48]. The vertical bar indicates the $Q_2(26.5)$ transition of NO. a/ at 1 mm and $T = 800$ K. b/ 22 mm and 2100 K.

found up to 225.2 nm (Fig. 5a). In particular, the position and relative intensities of the two bumps at 224 and 224.6 nm are correct. On the other hand, a difference of a factor 2 between the experimental and calculated cross sections is found at higher wavelengths, indicating some failure of the simulation, due to the lack of spectroscopic information. Using Eq. (2), the derived NH_3 mole fraction is 0.31 at 1 mm, which is reasonable considering that the NH_3 mole fraction in the mixture of the F3 flame is 0.48. In the burned gases the agreement between the spectra is less good (Fig. 5b). The simulated position of the second bump is too red-shifted and the relative intensity between the two bumps is not as well described, confirming that the lack of spectroscopic information has a greater impact at high temperature. The derived NH_3 mole fraction is found to be 0.19, at least one order of magnitude higher than the kinetic modeling results (not presented here). Note that these values are extracted after neglecting the absorbance due to the surrounding gases, and considering that the absorption pathlength is equal to 6 cm. No indication of NO or NH_3 contribution from surrounding gases is observed in the F3 flame (Figs. 3 and 12).

The simulation of the NH_3 absorption spectrum allows to identify that the absorbance signal collected in this work is due to NH_3. Further spectroscopic analysis is still required to extract the T-dependency of the absorption cross section in this wavelength range, and eventually extract the NH_3 density profile from absorbance measurements reported in Fig. 3a (open symbols). Improvements of the simulation are expected by considering the level ν_4 of the ground state. Indeed, it allows to fit new features observed above 220 nm at room T in [46] and to improve the agreement with the spectrum measured at $T = 595$ K in [37]. However, as discussed in the Supplementary Materials (SM-B-d), there is no data to calculate the oscillator strengths of the transition from this level which prevents us from going any further.

4.1.2. NO absorption

In the leanest flame F1, the absorbance spectra measured at different heights above the burner clearly evidence the contribution of NO absorption as shown in Fig. 6. The peaks correspond to the structured NO absorption spectrum and were observed only in the lean flame in which the highest amounts of NO are produced. The baseline of the absorbance spectrum measured at 25 mm is close to 0, indicating that NO species are the only species contributing to the absorbance, in agreement with the previous statements shown in Fig. 3. At 3 mm, there is an additional contribution of absorbance due to NH_3 as the baseline of the absorbance spectra increases to 30 % at 225.53 nm. The baseline of the spectra collected at 3 mm slightly decreases with the wavelength increase, in agreement with the magnification shown in Fig. 4. Note that the results presented in Fig. 3 were obtained after accumulating LIF signals over 300 laser shots at a given wavelength, and those reported in Fig. 6 were obtained from an accumulation of 10 laser shots during the wavelength scanning at a rate of 0.5 pm/s, yielding in a wider scattering of the data. The relative variation of the peak of each line between 3 and 25 mm is

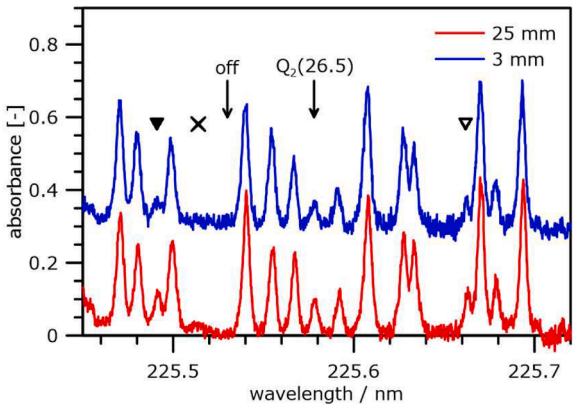

Fig. 6. Absorbance spectra measured in the lean flame F1 at HAB = 3 and 25 mm. The arrows indicate the $Q_2(26.5)$ transition of NO and the off-resonance wavelength. $Q_2(27.5)$ and $Q_2(25.5)$ transitions of NO are marked with closed and open triangles, respectively. $P_2(34.5)$ transition is marked with × symbol (see Section 4.3.2 and Fig. 13).

within ± 15% except for lines $Q_2(27.5)$ and $Q_2(25.5)$ (for which the variation is greater), both of which are partially overlapped by adjacent strong line. The NO absorbance along the $Q_2(26.5)$ transition is equal to 9 % (derived from the on – off-resonance measurements) at 25 mm, in agreement with the measurements shown in Fig. 3b, and is 8 % at 3 mm. From this observation, we conclude that the absorbance is mainly due to the NO species present in the surrounding gases, and that the composition of the surrounding gases is the same at both HABs.

As shown by Pillier et al. [40] in case of NO species, interpretation of absorption measurements is complex when the gas surrounding the flame contribute to additional absorption. Corrections for T and density along the radial axis are required. These corrections depend also on the selected rotational transitions; the lowest J" absorb stronger at cold T. Similarly, in the richest flames, NH_3 species are also among the possible absorbing species in the gases surrounding the flame. But as the NH_3 spectrum is broadband, its absorbance will only affect the baseline independently of the wavelength (in a restricted range).

Finally, we identified that NO and NH_3 species are responsible of the background absorption. This absorbance affects the effective laser intensity available at the center part of the flame that has to be quantified to correct the LIF signal according to Eq. (3). It was determined using the average signals of the 2 photodiodes located before and after the burner enclosure as explained in Section 3.2.

4.2. NO profiles

LIF signals were measured at the temporal peak along the flame axis

in all flames. LIF signals were corrected for the effective laser intensity available at the center of the flame (I_L) from the absorption measurements (Eq. (3)). As an illustration, Fig. 7 shows the prompt-LIF signals corrected for the laser intensities, I_L (on the burner axis) or I_0 (before the burner), as a function of HAB in case of the rich flame F3. The correction for I_0 considers only the fluctuations of the laser energy that are unavoidable with such laser source (diamond symbols). By contrast, the one with I_L considers the effective laser intensity along the flame axis due to the laser absorbance (discussed above), which leads to a substantial modification of the relative LIF profile. Thus, a 17% increase of the LIF signal (and thus of $N_{J''}$) is observed at 5 mm. Assuming that the prompt-LIF measurement is not affected by the variation of the fluorescence quantum yield (see Section A of the SM), the profile of relative rotational population of NO, $N_{J''}$, is derived directly from the corrected LIF signal profile (circle symbols), with an accuracy estimated to 7 %. It was found that the fluorescence decay rates measured along the HAB, remain constant in the burned gases (HAB > 5 mm) and equal to around 10^8 s^{-1} in all flames.

The relative rotational population of NO profiles were measured independently in all flames. Then, measurements of the corrected LIF signals were performed alternatively between the three flames at HAB = 20 mm in order to obtain the relative $N_{J''}$ at this HAB. Particular attention was paid to the effective laser intensity available at the center of the flame not only along the vertical axis but also during the switch between flames. Fig. 8 shows the relative rotational population $N_{J''}$ measured in all flames in arbitrary unit. The rotational population increases sharply in the first 5 mm above the burner. In the burned gases, the rotational population of NO of the F3 flame is found comparatively weak but with a SNR ~ 100. In the F1 flame, the rotational population reaches a plateau while it decreases slightly in the F2 flame. It should be noted that knowledge of the NO concentration in the flame is useless to proceed to the correction of the raw LIF profiles. Only the attenuation of the laser intensity is required at this stage. The accuracy of the relative rotational population was estimated to be equal to 12 %.

4.3. LIF thermometry

This section presents the methodology of the LIF thermometry used in this work. However, in the case of the lean F1 flame, the NO absorbance shown in Fig. 6 prevents the direct T measurements. As will be shown in Section 4.3.2, the experimental setup was modified to restrict its contribution.

4.3.1. Methodology

NO-LIF thermometry was conducted by tuning the wavelengths from 225.45 to 225.72 nm. Prompt-LIF signals and transmittance along the laser axis were recorded in order to correct the LIF signal from the laser intensity at the center of the flame. In case of the F2 and F3 flames, the absorbance spectra measured in this restricted range of wavelength (less than 0.3 nm) vary quasi linearly as function of the wavelength. In this wavelength range, the NH_3 absorbance decreases with the increase of wavelength by 15 % at 22 mm and by 26 % at 1 mm above the burner (see insert of Fig. 4). Fig. 9 shows the excitation NO-LIF spectrum obtained in the F2 flame at 20 mm and the transmittance (I_t/I_0). The transmittance spectrum indicates that there is a slight variation of the laser intensity, I_L, as a function of the wavelength, but without structured absorption. Thus, the LIF signal was only corrected for the small fluctuations of the laser intensity occurring during the scan.

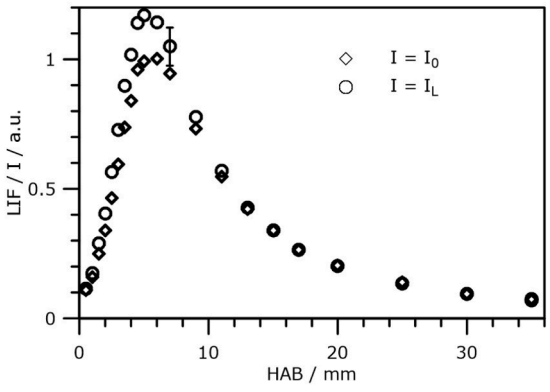

Fig. 7. LIF signals (corrected for the laser energy measured before the burner, I_0, or at the center of the flame, I_L,) as function of HAB in the rich flame F3.

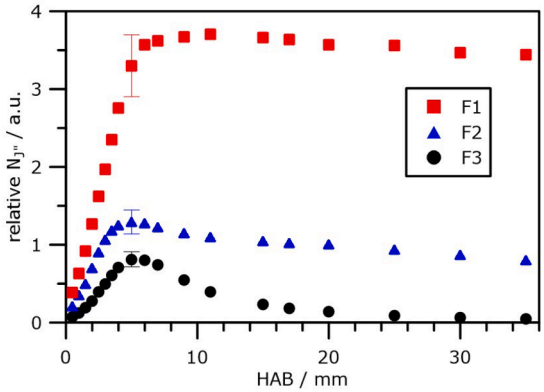

Fig. 8. Relative $N_{J''}$ population in flames $NH_3/O_2/N_2$ as function of HAB.

The LIF excitation spectrum was treated using thermo-NO-LIF software [19]. This software is a C++ program available in [44]. Fig. 10 shows an illustration of the best-fit simulated spectrum obtained using thermo-NO-LIF software. At 20 mm, temperature is equal to 1977 K in the F2 flame, and to 2089 K in the F3 flame. Temperature measurements were estimated with an accuracy of 5 %.

4.3.2. Specificity in the case of the lean flame, F1

In the F1 flame, temperature determination is confronted to the contribution of the surrounding NO absorbance as shown in Fig. 6. For instance, Fig. 11 shows the excitation LIF and the transmittance spectra measured at HAB = 25 mm. In that case where the absorbance due to species surrounding the flame is not only structured but T-dependent, the correction of the prompt-LIF signal for the variation of the laser intensity is not possible. Indeed, NO species, in the lowest J" rotational numbers, absorb stronger in the surrounding than at high temperature in the flame, in agreement with the Boltzmann distribution. Attempts were done to determine T from the LIF corrected for I_L spectrum but the best-fit procedure using thermo-NO-LIF software fails or gives erroneous values.

To overcome this problem and to reduce the influence of the absorption from gases surrounding the flame, two tubes were installed

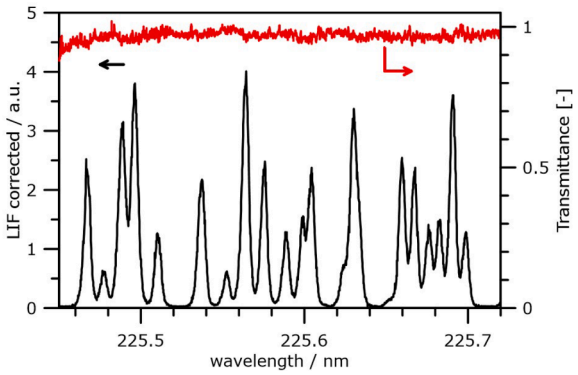

Fig. 9. LIF excitation and transmittance spectra in the F2 flame at 20 mm.

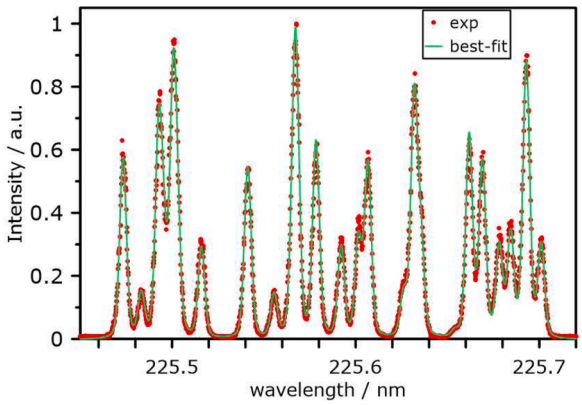

Fig. 10. Best-fit of NO-LIF spectrum in the F2 flame at 20 mm compared to the experimental one (correlation R^2=0.9936).

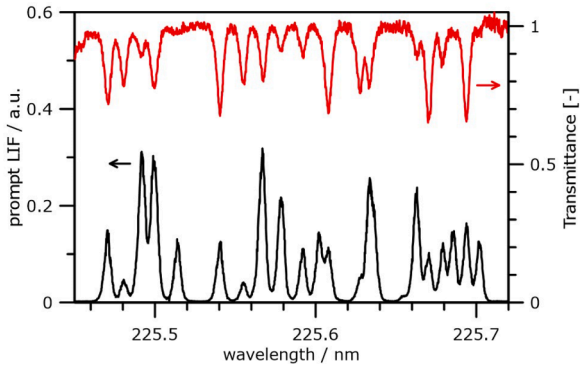

Fig. 11. LIF excitation and transmittance spectra in the F1 flame at 25 mm w/o tubes.

inside the burner along the laser axis, in a similar way as performed by Goldman et al. [45]. Each tube is 14 cm long and has an internal of diameter 6 mm. They are flushed with N_2 at low flow rate (50 sccm) to avoid disturbing the flame. With the tubes, the optical pathlength encompasses the 6-cm of flame and 7-cm of surrounding gases, reducing the absorbing pathlength from 41 to 13 cm, as shown in Fig. 2. This latter distance could not be any further reduced due to the burner's overall diameter (equal to 12 cm). Care was taken to ensure that neither the presence of tubes nor gas flushing disturbed the flame by controlling the NO LIF profiles with and without the tubes in the F1 flame. The $N_{J"}$ profile re-assessed in presence of the tubes, was found in very good agreement with the one obtained without the tubes, validating the method of the correction of the laser energy at the center of flame. In the F2 flame, where the absorbance was limited, temperature was also measured in presence of the tubes without any indication of variation of *T*.

When the laser wavelength is tuned at 225.53 nm (off-resonance of NO), absorbance profiles along the vertical axis of the flames were measured with the tubes. NH_3 absorbance measured in presence of the tubes, shown Fig. 12, are close to the ones previously measured without (open symbols shown in Fig. 3a). This clearly indicates that the NH_3 absorption measured without tube is due to the NH_3 present in the flame. Contrary to NO species that absorb at low temperature in the surrounding gases, NH_3 absorption is negligible at cold *T*.

Fig. 13 shows the prompt-LIF spectra measured at HAB = 25 mm in the F1 flame with (green curve) and without (black curve, also shown in Fig. 11) tubes inside the vessel. The LIF spectra are normalized at λ = 225.516 nm. It corresponds to the P_2+Q_{12}(34.5) transition, i.e. the highest J" number in this spectral range (identified with the × mark). Also, this transition is unaffected by absorbance along the laser axis (×

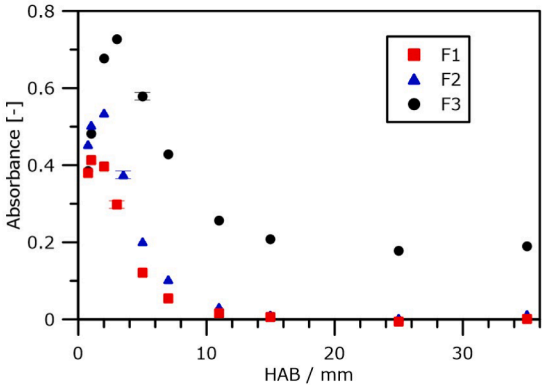

Fig. 12. NH_3 absorbance measured in $NH_3/O_2/N_2$ flames in presence of the tubes, see text. Error bar size is included in symbol size.

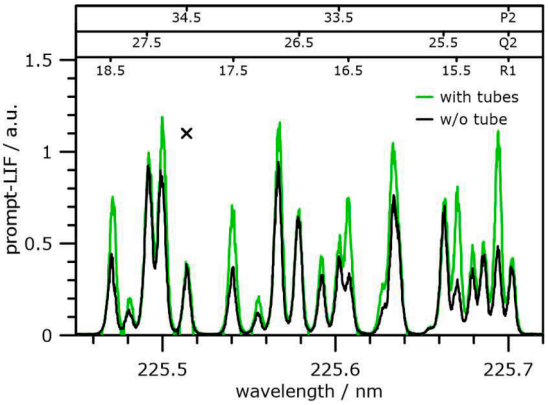

Fig. 13. LIF excitation and absorption spectra in the F1 flame at 25 mm with and without the tubes inside the enclosure. The × mark indicates P_2+Q_{12}(34.5) transition as used for the normalization of the spectra. The upper *X-axis* indicate the J" numbers of the P_2+Q_{12}, Q_2+R_{12} and R_1+Q_{21} transitions of NO.

mark in Fig. 6). The comparison of the LIF spectra clearly shows that without the tubes, the lower J" number, the higher decrease of the relative intensity of the prompt-LIF, relatively to the spectrum obtained with tubes. The decrease of the LIF signal reaches a factor of 2.0 for J" = 17.5, and 2.7 for J" = 15.5. Indeed, the absorbance of the lower J" number increases with the decrease of *T* (in the surrounding gases). The installation of the tube prevents the NO absorption from the surrounding gases in the F1 flame. Thus, it was possible to correct the LIF signal from the variation of the laser intensity as performed in the previous section. Finally, the implementation of the tubes in the enclosure allowed to determine *T* using thermo-NO-LIF software along the HAB of the F1 flame without additional difficulty. At 25 mm in the F1 flame, *T* was found to be equal to 1820 K.

5. Conclusions

NO-LIF measurements were carried out in low-pressure ammonia flat flames in order to measure both NO species and temperature profiles along the vertical axis. NO is excited along the $A^2\Sigma^+$-$X^2\Pi$(0,0) band around 225 nm, and the fluorescence is collected at 245 nm along the $A^2\Sigma^+$-$X^2\Pi$(0,2) band. Measurements were performed in the linear regime of LIF. LIF signals were therefore corrected for laser intensity at the center of the flame. NO profiles were obtained by probing the Q_2(26.5) transition. NO-LIF thermometry was performed to determine *T* from experimental spectrum obtained by scanning the wavelength from 225.45 to 225.72 nm.

The present work highlights absorbance along the laser axis in the

burner enclosure. Measurements were conducted at the $Q_2(26.5)$ transition of NO and after detuning wavelength off-resonance. Absorbances as high as 70 % were obtained near the burner surface. There were identified as being due to NH_3 species, which has a quasi-continuum absorption spectrum, and to NO, which has a structured absorption spectrum. The high levels of concentration of NO and/or NH_3 present in the flame are spread into the surrounding gases of these confined flames. It is reported that the species absorbance, due to NO, in the surrounding gases was nearly independent of the HAB. NH_3 absorbance is mostly due to the NH_3 species present in the flame, as the measurements performed after installing tubes along the laser axis prevents NO absorbance but not NH_3 absorbance. Indeed, as shown from the spectral simulation, the NH_3 absorption cross section around 225.5 nm (transitions from the level $2\nu_2$ of the ground state) increases sharply with *T*. However, the NH_3 spectroscopy at high *T* still suffers from a lack of data to extract the NH_3 species concentration profiles using absorption. Further high-temperature measurements and spectroscopic analysis are needed to improve the accuracy of the NH_3 cross-section simulation for *in situ* NH_3 quantification.

NO-LIF profiles, corrected for the laser intensity variations, were measured as a function of the HAB in the premixed flames. In the rich and near-stoichiometric flames, temperature was measured using NO-LIF thermometry. *T* was derived from NO-LIF spectrum treated with the thermo-NO-LIF software. However, in the leanest flame, the wavelength-dependent absorbance of the surrounding gases, due to NO species, prevents temperature determination from the NO-LIF spectrum measurement. To overcome this problem, 2 tubes flushed with N_2, were installed in the chamber to reduce the absorption pathlength. As a result, temperature determination was finally obtained from NO-LIF spectrum measurements. The present strategy is currently being applied to measure NO mole fraction and *T* profiles in different low-pressure ammonia flames. The procedure can be extended to any stationary flame at any pressure. Stationarity is preferable to evaluate the background absorption due to NH_3 and NO. An additional correction for quenching variations will be necessary at high pressure.

The $A^2\Sigma^+$-$X^2\Pi(0,0)$ band was selected in this work because of the need to evaluate the NO-LIF thermometry in ammonia flames. In case NO concentration fields are the only interest, the $A^2\Sigma^+$-$X^2\Pi(0,1)$) band at 236 nm is an interesting option, because much less confronted to background absorption (NH_3 and/or NO), even though measurements are 1/ much more sensitive to the temperature and 2/ affected by a much lower signal intensity.

Further measurements will be performed in order to quantify the NO profiles in absolute mole fraction. Also, knowing the temperature profiles, kinetic modeling calculations will be conducted to evaluate the predicted NO using different kinetic models available in the literature.

Novelty and significance statement

In this study, we elucidate the absorption contribution not only from NH_3 but also from NO in confined low-pressure $NH_3/O_2/N_2$ flames. It is shown that at around 225 nm, the absorption is due the lowest J" rotational numbers of NO surrounding the flame that absorb strongly at low *T*, and to high vibrational band of NH_3 present in the flame. This absorption affects the NO-LIF measurements performed to measure both the NO profiles and *T* profiles using NO-LIF thermometry. The strategy developed in the present work allows to overcome these difficulties.

Supporting Information: supplementary materials 1/ "details on prompt-LIF measurements and on NH3 spectroscopy", 2/ "PGOPHER file"

CRediT authorship contribution statement

Nour El Baba: Methodology, Formal analysis, Data curation. **Pascale Desgroux:** Supervision, Project administration, Writing – review & editing. **Nathalie Lamoureux:** Supervision, Project administration, Writing – review & editing.

Declaration of competing interest

The authors declare that they have no known competing financial interests or personal relationships that could have appeared to influence the work reported in this paper.

Acknowledgments

This work is a contribution to the ANR SIAC (ANR-22-CE50-0022) and the LabEx CaPPA (ANR-11-LABX-0005-01) projects funded by the French National Research Agency, to MéOL plateforme of Univ. Lille, and to the CPER research project ECRIN funded by the French Ministère de l'Enseignement Supérieur et de la Recherche. The authors thank the Regional Council "Hauts-de-France" and the "European Regional Development Fund", and the French Agency for Ecological Transition (ADEME) for their financial support to this project.

Supplementary materials

Supplementary material associated with this article can be found, in the online version, at doi:10.1016/j.combustflame.2024.113424.

References

[1] A.R. Ravishankara, J.S. Daniel, R.W. Portmann, Nitrous oxide (N_2O): the dominant ozone-depleting substance emitted in the 21st century, Science 326 (2009) 123–125.
[2] H.O.T. Pye, A. Nenes, B. Alexander, A.P. Ault, M.C. Barth, S.L. Clegg, J. L. Collett Jr., K.M. Fahey, C.J. Hennigan, H. Herrmann, M. Kanakidou, J.T. Kelly, I. T. Ku, V.F. McNeill, N. Riemer, T. Schaefer, G. Shi, A. Tilgner, J.T. Walker, T. Wang, R. Weber, J. Xing, R.A. Zaveri, A. Zuend, The acidity of atmospheric particles and clouds, Atmos. Chem. Phys. 20 (2020) 4809–4888.
[3] K.P. Shrestha, C. Lhuillier, A.A. Barbosa, P. Brequigny, F. Contino, C. Mounaïm-Rousselle, L. Seidel, F. Mauss, An experimental and modeling study of ammonia with enriched oxygen content and ammonia/hydrogen laminar flame speed at elevated pressure and temperature, Proc. Combust. Inst. 38 (2021) 2163–2174.
[4] X. Zhang, S.P. Moosakutty, R.P. Rajan, M. Younes, S.M. Sarathy, Combustion chemistry of ammonia/hydrogen mixtures: jet-stirred reactor measurements and comprehensive kinetic modeling, Combust. Flame 234 (2021) 111653.
[5] K.N. Osipova, X. Zhang, S.M. Sarathy, O.P. Korobeinichev, A.G. Shmakov, Ammonia and ammonia/hydrogen blends oxidation in a jet-stirred reactor: experimental and numerical study, Fuel 310 (2022) 122202.
[6] P. Sabia, M.V. Manna, A. Cavaliere, R. Ragucci, M. de Joannon, Ammonia oxidation features in a jet stirred flow reactor. The role of NH_2 chemistry, Fuel 276 (2020) 118054.
[7] M.S. Chou, A.M. Dean, D. Stern, Laser absorption measurements of OH, NH, and NH_2 in NH_3/O_2 flames: determination of an oscillator strength for NH_2, J. Chem. Phys. 76 (1982) 5334–5340.
[8] M. Chou, A.M. Dean, D. Stern, Laser induced fluorescence and absorption measurements of NO in NH_3/O_2 and CH_4/air flames, J. Chem. Phys. 78 (1983) 5962–5970.
[9] J. Bian, J. Vandooren, P.J. Van Tiggelen, Experimental study of the structure of an ammonia-oxygen flame, Symp. Int. Combust. 21 (1986) 953–963.
[10] J. Vandooren, J. Bian, P.J. Van Tiggelen, Comparison of experimental and calculated structures of an ammonia-nitric oxide flame. Importance of the NH_2 + NO reaction, Combust. Flame 98 (1994) 402–410.
[11] C. Duynslaegher, H. Jeanmart, J. Vandooren, Flame structure studies of premixed ammonia/hydrogen/oxygen/argon flames: experimental and numerical investigation, Proc. Combust. Inst. 32 (2009) 1277–1284.
[12] C. Brackmann, V.A. Alekseev, B. Zhou, E. Nordström, P.E. Bengtsson, Z. Li, M. Aldén, A.A. Konnov, Structure of premixed ammonia + air flames at atmospheric pressure: laser diagnostics and kinetic modeling, Combust. Flame 163 (2016) 370–381.
[13] S. Colson, Y. Hirano, A. Hayakawa, T. Kudo, H. Kobayashi, C. Galizzi, D. Escudié, Experimental and numerical study of NH_3/CH_4 counterflow premixed and non-premixed flames for various NH_3 mixing ratios, Combust. Sci. Technol. 193 (2020) 1–18.
[14] K.N. Osipova, O.P. Korobeinichev, A.G. Shmakov, Chemical structure and laminar burning velocity of atmospheric pressure premixed ammonia/hydrogen flames, Int. J. Hydrog. Energy 46 (2021) 39942–39954.
[15] K.N. Osipova, S.M. Sarathy, O.P. Korobeinichev, A.G. Shmakov, Chemical structure of premixed ammonia/hydrogen flames at elevated pressures, Combust. Flame 246 (2022) 112419.
[16] H. Tang, C. Yang, G. Wang, T.F. Guiberti, G. Magnotti, Raman spectroscopy for quantitative measurements of temperature and major species in high-pressure non-premixed $NH_3/H_2/N_2$ counterflow flames, Combust. Flame 237 (2022) 111840.

[17] D. Zhu, Z. Qu, M. Li, S. Agarwal, R. Fernandes, B. Shu, Investigation on the NO formation of ammonia oxidation in a shock tube applying tunable diode laser absorption spectroscopy, Combust. Flame 246 (2022) 112389.

[18] D. Zheng, D. He, Y. Du, J. Li, M. Zhang, Y. Ding, Z. Peng, Experimental study of the methane/hydrogen/ammonia and ethylene/ammonia oxidation: multi-parameter measurements using a shock tube combined with laser absorption spectroscopy, Combust. Flame 254 (2023) 112830.

[19] K.K. Foo, N. Lamoureux, A. Cessou, C. Lacour, P. Desgroux, The accuracy and precision of multi-line NO-LIF thermometry in a wide range of pressures and temperatures, J. Quant. Spectrosc. Radiat. Transf. 255 (2020) 107257.

[20] A.T. Hartlieb, B. Atakan, K. Kohse-Höinghaus, Temperature measurement in fuel-rich non-sooting low-pressure hydrocarbon flames, Appl. Phys. B 70 (2000) 435–445.

[21] W.G. Bessler, C. Schulz, T. Lee, J.B. Jeffries, R.K. Hanson, Strategies for laser-induced fluorescence detection of nitric oxide in high-pressure flames. I. A-X(0, 0) excitation, Appl. Opt. 41 (2002) 3547–3557.

[22] W.G. Bessler, C. Schulz, T. Lee, J.B. Jeffries, R.K. Hanson, Strategies for laser-induced fluorescence detection of nitric oxide in high-pressure flames. II. A-X(0, 1) excitation, Appl. Opt. 42 (2003) 2031–2042.

[23] W.G. Bessler, C. Schulz, T. Lee, J.B. Jeffries, R.K. Hanson, Strategies for laser-induced fluorescence detection of nitric oxide in high-pressure flames. III. Comparison of A-X excitation schemes, Appl. Opt. 42 (2003) 4922–4936.

[24] D.D. Thomsen, F.F. Kuligowski, N.M. Laurendeau, Background corrections for laser-induced-fluorescence measurements of nitric oxide in lean, high-pressure, premixed methane flames, Appl. Opt. 36 (1997) 3244–3252.

[25] C.S. Cooper, N.M. Laurendeau, Parametric study of NO production via quantitative laser-induced fluorescence in high-pressure, swirl-stabilized spray flames, Proc. Combust. Inst. 28 (2000) 287–293.

[26] J.R. Reisel, Modeling of nitric oxide formation in high-pressure premixed laminar ethane flames, Combust. Flame 120 (2000) 233–241.

[27] N. Lamoureux, H. El Merhubi, L. Pillier, S. de Persis, P. Desgroux, Modeling of NO formation in low pressure premixed flames, Combust. Flame 163 (2016) 557–575.

[28] J.K. Dixon, The ultraviolet absorption bands of ammonia, Phys. Rev. 43 (1933) 711–715.

[29] A.D. Walsh, P.A. Warsop, The ultra-violet absorption spectrum of ammonia, Trans. Faraday Soc. 57 (1961) 345–358.

[30] M. Versluis, N. Georgiev, L. Martinsson, M. Aldén, S. Kröll, 2-D absolute OH concentration profiles in atmospheric flames using planar LIF in a bi-directional laser beam configuration, Appl. Phys. B 65 (1997) 411–417.

[31] Q. Fan, X. Liu, X. Cai, C. Brackmann, M. Aldén, X.S. Bai, Z. Li, Structure and scalar correlation of ammonia/air turbulent premixed flames in the distributed reaction zone regime, Combust. Flame 241 (2022) 112090.

[32] B. Cosway, P. Ahmed, M. Talibi, R. Balachandran, Inverstigation of NO production and flame structures in ammonia-hydrogen flames, J. Ammon. Energy 1 (2023) 106–117.

[33] G. Wang, H. Tang, C. Yang, G. Magnotti, W.L. Roberts, T.F. Guiberti, Quantitative laser-induced fluorescence of NO in ammonia-hydrogen-nitrogen turbulent jet flames at elevated pressure, Proc. Combust. Inst. 39 (2023) 1465–1474.

[34] P. Jamette, V. Ricordeau, B. Deschamps, P. Desgroux, Laser induced fluorescence detection of NO in the combustion chamber of an optical GDI engine with A-X(0,1) excitation, in: Proceedings of the International Spring Fuels & Lubricants Meeting, SAE International, 2001.

[35] A.M. Dean, M.S. Chou, D. Stern, Kinetics of rich ammonia flames, Int. J. Chem. Kinet. 16 (1984) 633–653.

[36] X. Yang, Z. Peng, Y. Ding, Y. Du, Spatially resolved broadband absorption spectroscopy measurements of temperature and multiple species (NH, OH, NO, and NH_3) in atmospheric-pressure premixed ammonia/methane/air flames, Fuel 332 (2023) 126073.

[37] W. Weng, S. Li, M. Aldén, Z. Li, Ultraviolet absorption cross-sections of ammonia at elevated temperatures for nonintrusive quantitative detection in combustion environments, Appl. Spectrosc. 75 (2021) 1168–1177.

[38] T.M. Rault, S. Clees, M. Figueroa-Labastida, S.C. Barnes, A.M. Ferris, N. Obrecht, C. Callu, R.K. Hanson, Multi-speciation and ignition delay time measurements of ammonia oxidation behind reflected shock waves, Combust. Flame 260 (2024) 113260.

[39] V.A. Lozovsky, I. Rahinov, N. Ditzian, S. Cheskis, Laser absorption spectroscopy diagnostics of nitrogen-containing radicals in low-pressure hydrocarbon flames doped with nitrogen oxides, Faraday Discuss. 119 (2002) 321–335.

[40] L. Pillier, C. Moreau, X. Mercier, J.F. Pauwels, P. Desgroux, Quantification of stable minor species in confined flames by cavity ring-down spectroscopy: application to NO, Appl. Phys. B. 74 (2002) 427–434.

[41] N. Lamoureux, P. Desgroux, A. El Bakali, J.F. Pauwels, Experimental and numerical study of the role of NCN in prompt-NO formation in low-pressure $CH_4/O_2/N_2$ and $C_2H_2/O_2/N_2$ flames, Combust. Flame 157 (2010) 1929–1941.

[42] P. Desgroux, L. Gasnot, J.F. Pauwels, L.R. Sochet, Correction of LIF temperature measurements for laser absorption and fluorescence trapping in a flame–application to the thermal perturbation study induced by a sampling probe, Appl. Phys. B Laser Opt. 61 (1995) 401–407.

[43] M.D. Sylla, N. Lamoureux, L. Gasnot, Impact of methyl butanoate oxidation on NO formation in laminar low pressure flames, Fuel 207 (2017) 801–813.

[44] K.K. Foo, N. Lamoureux, P. Desgroux, Software thermo NO-LIF, (2020), https://pc2a.univ-lille.fr/thermo-no-lif/.

[45] A. Goldman, I. Rahinov, S. Cheskis, Molecular oxygen detection in low pressure flames using cavity ring-down spectroscopy, Appl. Phys. B 82 (2006) 659–663.

[46] P. Limão-Vieira, N.C. Jones, S.V. Hoffmann, D. Duflot, M. Mendes, A.I. Lozano, F. Ferreira da Silva, G. García, M. Hoshino, H. Tanaka, Revisiting the photoabsorption spectrum of NH_3 in the 5.4–10.8 eV energy region, J. Chem. Phys. 151 (2019) 184302.

[47] P.G. Menon, K.W. Michel, Ultraviolet absorption of ammonia at high temperatures behind shock waves, J. Phys. Chem. 71 (1967) 3280–3284.

[48] C.M. Western, PGOPHER: a program for simulating rotational, vibrational and electronic spectra, J. Quant. Spectrosc. Radiat. Transf. 186 (2017) 221–242.

[49] X. Huang, D.W. Schwenke, T.J. Lee, Rovibrational spectra of ammonia. II. Detailed analysis, comparison, and prediction of spectroscopic assignments for $^{14}NH_3$, $^{15}NH_3$, and $^{14}ND_3$, J. Chem. Phys. 134 (2011) 044321.

[50] W. Weng, Z. Li, Private communication, (2023).

[51] W.S. Benedict, E.K. Plyler, Vibration-rotation bands of ammonia: II. The molecular dimensions and harmonic frequencies of ammonia and deutered ammonia, Can. J. Phys. 35 (1957) 1235–1241.

[52] J.C. Pearson, S. Yu, O. Pirali, Modeling the spectrum of the $2\nu_2$ and ν_4 states of ammonia to experimental accuracy, J. Chem. Phys. 145 (2016) 124301.

[53] L.D. Ziegler, Rovibronic absorption analysis of the $\tilde{A} \leftarrow \tilde{X}$ transition of ammonia, J. Chem. Phys. 82 (1985) 664–669.

[54] W.R. Harshbarger, Franck–Condon Factors for the $\tilde{A} \leftarrow \tilde{X}$ transition of ammonia with anharmonic potential functions for the ground and excited states, J. Chem. Phys. 53 (2003) 903–911.

[55] B. Cheng, H. Lu, H. Chen, M. Bahou, Y. Lee, A.M. Mebel, L.C. Lee, M. Liang, Y. L. Yung, Absorption cross sections of NH_3, NH_2D, NHD_2, and ND_3 in the spectral range 140–220 nm and implications for planetary isotopic fractionation, Astrophys. J. 647 (2006) 1535–1542.

[56] N. Lamoureux, C.M. Western, X. Mercier, P. Desgroux, Reinvestigation of the spectroscopy of the $\tilde{A}^3\Pi_u$-$\tilde{X}^3\Sigma_g^-$ transition of the NCN radical at high temperature: application to quantitative NCN measurement in flames, Combust. Flame 160 (2013) 755–765.

[57] X. Zhu, J. Ma, D.R. Yarkony, H. Guo, Computational determination of the $\tilde{A}$ state absorption spectrum of NH_3 and of ND_3 using a new quasi-diabatic representation of the $\tilde{X}$ and $\tilde{A}$ states and full six-dimensional quantum dynamics, J. Chem. Phys. 136 (2012) 234301.